CERN – EUROPEAN ORGANIZATION FOR NUCLEAR RESEARCH

CLIC – Note – 1171

NEW OPTIMIZED FULLY LOADED CLIC DRIVE BEAM ACCELERATING STRUCTURE DESIGN

Ana Dorda Martín, Steffen Doebert

CERN, Geneva, Switzerland

CERN-ACC-2021-0003
20/05/2021

Abstract

The CLIC drive beam accelerator (DBA) provides a very high current beam to supply the RF power to the main accelerator; therefore, its efficiency is the most important figure of merit. The travelling wave SICA (Slotted Iris – Constant Aperture) structures of CLIC DBAs accelerate the drive beam to 2.37 GeV. Recent updates of the CLIC parameters made a revision of the original design necessary. We optimized and redesigned the structure to match the new input power of 18.00 MW, keeping the RF to beam efficiency over 95 % and a filling time of 245.00 ns. Higher-Order Modes (HOMs) can be excited by the beam due to the large beam current of 4.21 A, despite the heavy damping by the slotted irises. We studied in detail the HOM to prove their damping accomplished by the SiC loads. Finally, we illustrate a design of the couplers. RF-kicks from the couplers have been studied using the beam dynamics code PLACET.

Geneva, Switzerland
20 May 2021

1 Introduction

The CLIC scheme is based in a two beam system where the Drive Beam (DB) gives the necessary energy for the collision to the Main Beams. For the nominal design of CLIC (which is supposed to reach a centre of mass of 3.00 TeV) it is planned to use two identical Drive Beam Accelerators (DBAs). Each of them will accelerate a DB to 2.37 GeV. Due to the large beam current of 4.21 A, Higher Order Modes (HOMs) may be excited by the beam leading to beam breakup or emittance growth.

For the previous design of DBA's accelerating structures, different structure types were considered [1]. After discarding the down-scaled version of the Tapered Damped Structure (TDS) used in the CLIC main beam accelerator due to its enormous size working at 1.00 GHz, the Slotted Iris-Constant Aperture (SICA) type was chosen [2]. This SICA structure detunes the dipole modes along the structure in addition to the slots, helping to suppress the HOMs further. This detuning is possible thanks to different size nose cones in every cell, and short range wakefields are reduced by the constant beam aperture along the structure. All the cells are iris slotted in four quadrants and every slot guides dipoles and quadruple modes into SiC loads, damping them. The concept has been used already in the CLIC Test Facility at 3 GHz successfully, proving its damping properties and efficiency [3, 4].

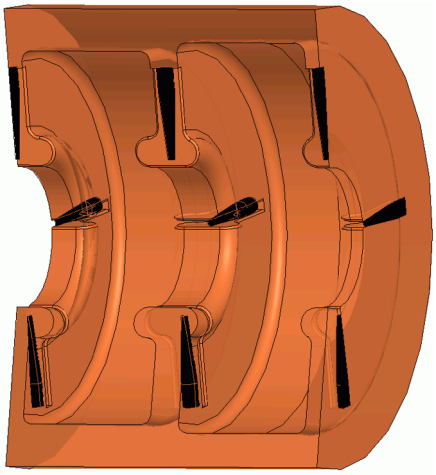

Figure 1: *First 2 cells of the travelling wave structure. The SiC loads for damping the HOM are black colored.*

The SICA type travelling wave (TW) structure that we will be optimizing and redesigning was arranged to work at a frequency of 999.50 MHz with an input power of 15.00 MW. The filling time of the structure was matched to 245±5 ns, so the frequency components of 4.00 MHz and multiples, included in the noise generated by the RF amplifier, are band-stopped. Those noise components are dangerous for the beam as they can be added up later during the bunch combination scheme of the drive beam generation. Furthermore, the RF to beam efficiency reached the desired value of 95 %.

Recent updates of the CLIC parameters made a revision of the original design necessary. The power given by the klystrons to the accelerating structures has increased to 20.00 MW. After passing through the coupling waveguides, the RF input power at the SICA structures is 18.00 MW [5]. Taking into account the beam dynamic simulations performed to find a compromise between beam aperture and

structure length that were performed for the 15.00 MW design, the number of cells has been increased from 19 to 21; keeping the same requirement of RF to beam efficiency over 95 % and a filling time of 245±5 ns. HOMs have been newly studied and a design of the couplers has been done. In addition the influence of the residual dipole field componenst in the coupler on hte beam has been studied with PLACET [6]

2 Structure optimization

During the design of the SICA structure for 15 MW input power, several beam dynamics simulations were performed. The objective of these simulations was to optimize both the beam aperture and the length of the structure, reaching a group velocity per cell that makes the structure match the requirements of RF to beam efficiency over 95 % and a filling time of 245±5 ns. The final values for the beam aperture (diameter) and number of cells were 98.00 mm and 19 cells.

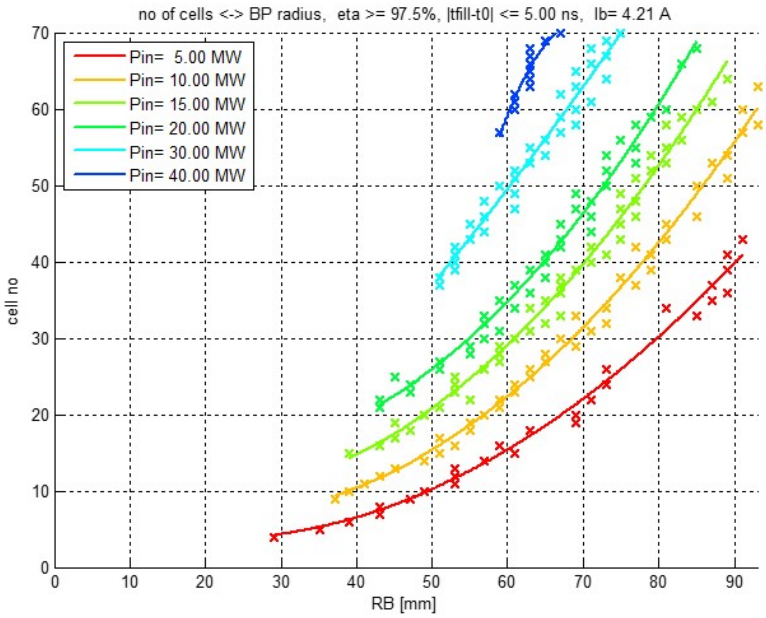

Figure 2: *Graphic extracted from [7]. For every input power a beam aperture and a number of cells, together with a group velocity, can be chosen to match the requirements.*

With the objective to keep the same beam aperture, and taking into account the proportional relation between the number of cells and the square root of the input power shown in [8], the optimum number of cells for an input RF power of 18.00 MW is 21 cells; which matches with the results obtained from the beam dynamic simulations as can be seen in Fig. 2.

As we only knew the dimensions of the structure with 19 cells, in order to keep a similar group velocity, was needed to perform an escalation of the main dimensions of the structure for 21 cells. These are the radius of the cell (R_a), the nose cone length (L_a) and the gap. This escalation was performed with two different methods, as shown in Fig. 3b. Method 1 is based on curve fitting, where one has a parametric

model function and wants to adjust the numerical values for the model so that it matches the data. On the other hand, method 2 is based on interpolation, which allows us to predict values at unknown points from values of known points. Finally method 2 was preferred as the group velocity per cell was more close to the one of the structure with 19 cells.

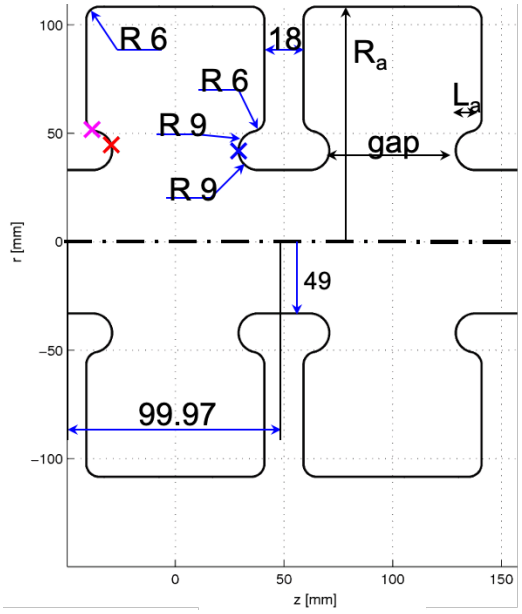

(a) *Dimensions of the first two cells. Blue arrows determine the fixed values in every cell while R_a, L_a and gap change their values along every cell of the structure.*

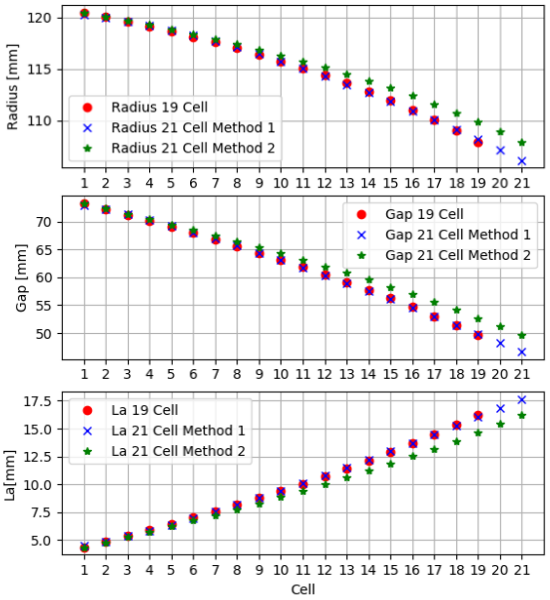

(b) *Comparison of the two methods of escalation of R_a, L_a and gap with the current values of the structure with 19 cells. The so called Method 1 corresponds with curve fitting while Method 2 with interpolation.*

Figure 3: *Process of escalation of the sizes R_a, L_a and gap of the structure with 19 cells to 21 cells.*

Once we knew the cell dimensions of the structure with 21 cells, it was necessary to check that the requirements of filling time and RF to beam efficiency continued being accomplished. To do that, taking into account the principle of energy conservation, we proceeded to model the multi cell travelling wave structure behaviour.

The input voltage $V_{in,1}$ of the first cell can be described as

$$V_{in,1} = P_{in}\sqrt{\frac{R/Q_1 w_0 L_1}{v_{gr,1}}} \tag{1}$$

where P_{in} is the input power at the beginning of the structure and R/Q_1, L_1 and $v_{gr,1}$ are the value of R/Q, the length and the group velocity at the first cell respectively. In our structure, the value of the length of every cell L_n keeps the value 99.98 mm. The relation between the input voltage $V_{in,n}$ and the output voltage $V_{out,n}$ at any cell n is defined as

$$g_n(V_{in,n}^2 - V_{out,n}^2) = \frac{I_b}{2}(V_{in,n} + V_{out,n}) + \frac{1}{4R_n}(V_{in,n} + V_{out,n})^2, \tag{2}$$

where g_n is

$$g_n = \frac{v_{gr,n}}{R/Q_n L_n w_0}. \tag{3}$$

Replacing $(V_{in,n}^2 - V_{out,n}^2)$ by $(V_{in,n} + V_{out,n})(V_{in,n} - V_{out,n})$ in (2) we obtain the following equation to describe the dependency of the output voltage on the input voltage

$$V_{out,n} = \frac{V_{in,n}(1 - \frac{1}{4R_n g_n}) - \frac{I_b}{2g_n}}{1 + \frac{1}{4R_n g_n}}. \tag{4}$$

The input voltage on the next cell $V_{in,n+1}$ depending on the output voltage in the current cell $V_{out,n}$ can be calculated as follows

$$V_{in,n+1} = V_{out,n}\sqrt{\frac{v_{gr,n} R/Q_{n+1} L_{n+1}}{v_{gr,n+1} R/Q_n L_n}}. \tag{5}$$

Moving forward with the power flow along the structure, the output power of one cell $P_{out,n}$ related with the input power of that cell $P_{in,n}$ can be described as shown in (6). $P_{b,n}$ represents the RF power given to the beam and is related with its current (which in our case is 4.21 A) while $P_{d,n}$ is the power dissipated in the walls of the cell.

$$P_{out,n} = P_{in,n} - P_{b,n} - P_{d,n} \tag{6}$$

$$P_{b,n} = V_n \cdot I_b \tag{7}$$

$$P_{d,n} = \frac{V_n^2}{R_n} \tag{8}$$

Finally, the accelerating gradient $(E_0T)_n$ is defined as the relation between the average voltage in the cell V_n and the length of the cell. Both definitions, for the accelerating gradient and the average voltage, are shown in (9) and (10).

$$(E_0T)_n = \frac{V_n}{L_n} \tag{9}$$

$$V_n = \frac{1}{2} \cdot (V_{in,n} + V_{out,n}) \tag{10}$$

Taking all this into account, it was possible to optimize the group velocity of the structure with 21 cells. First of all, we simulated every cell from the escalated structure with HFSS. Doing this, we obtained the values of R/Q, Q and group velocity per cell. Using the above described behaviour of the structure, it was possible to obtain the values of filling time and RF to beam efficiency of the structure with escalated dimensions. Both of them are defined as

$$\eta = \frac{\sum_n P_{b,n}}{P_{in}} \tag{11}$$

$$t_{fill} = \sum_n \frac{L_n}{v_{gr,n}}. \tag{12}$$

The calculations demonstrated that a new tuning of the group velocity was required to reach the requirements of filling time and RF to beam efficiency. Therefore,

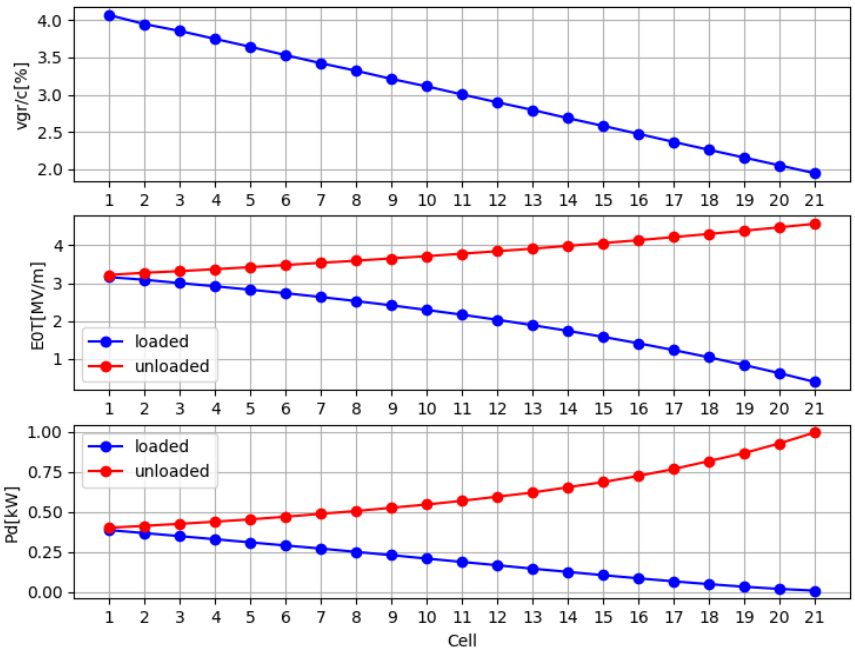

Figure 4: *Electromagnetic properties of the structure with 21 cells. Up: group velocity per cell in reference to the speed of light. Middle, accelerating gradient in the loaded (beam current of* 4.21 A*) and unloaded case. Bottom: dissipated power per cell in the loaded and unloaded case for an RF duty cycle of 75 %.*

using the values R/Q and Q per cell, we optimized the group velocity by adjusting the nose cones to reach the conditions.

At the end of the optimization process we obtained a structure of 21 cells with a beam aperture radius of 49.00 mm, and a total length of 2.30 m. The operating frequency of every cell was tuned to 999.50 MHz. The results of the tuning of the group velocity converged to an RF to beam efficiency of 99.37 % and a filling time of 244.67 ns. The group velocity decreases lineally along the structure as can be seen in Fig. 4. The power lost in each cell and the accelerating gradient per cell is also plotted in Fig. 4, being the red line the unloaded case and the blue line the loaded case with a beam current of 4.21 A.

3 HOM study

In order to study the reduction of the HOM by damping and detuning, we based the analysis in the comparison of three different parameters. R/Q is a parameter commonly used in RF cavity design [9] to quantify the interaction of the mode with the beam. It is related with the accelerating voltage and the energy stored in the cavity. $Q_{CavitySurface}$ is used to evaluate the losses in the cavity and is also related with the energy stored inside it and the power losses on its surface. Both R/Q and $Q_{CavitySurface}$ can be found using formula (13) and (14) respectively. By multiplying both of them together, we can obtain the shunt impedance R (which was previously used as R_n). The last parameter we are going to be using is Q_{SiC}, which is defined

as the $Q_{CavitySurface}$ but in this case is refer to the SiC loads.

$$R/Q = \frac{|V_{acc}|^2}{wW_e} \tag{13}$$

$$Q_{CavitySurface} = \frac{wW_e}{P_{loss}} \tag{14}$$

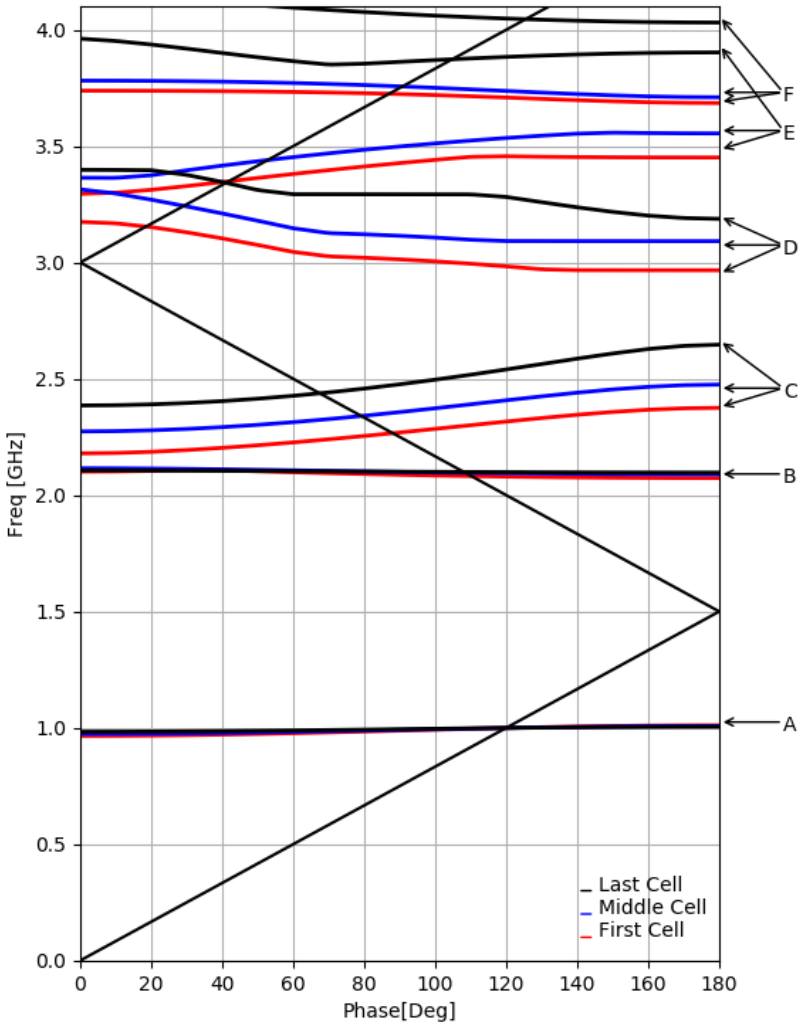

Figure 5: *Detuning curves: representation of the resonant frequency of the selected mode bands for the monopole modes as a function of the phase advance per cell.*

To obtain the frequency and phase advance of the HOM from HFSS simulations for three different cells.We plotted the *Brillouin Diagram* of the first 20 modes (see for example Fig. 5). This is a well-known method to analyse periodic structures [9] based on plotting the variation of the frequency of the modes of a periodic structure depending on the phase advance. Over these curves, we plot the speed of light line. At the points where this line crosses with the dispersion curve is when a particle at the speed of light is synchronous with the mode, thus seeing the correct phase in every cell. For example, in Fig. 5 we plotted the *Brillouin Diagram* for the modes of the first, middle and last cell that interact with the beam. If we focus on the operating mode (around 1.00 GHz in the plot) we can see that it crosses with the

speed of light line at $2\pi/3$, which is the design phase advance. So that, to study every HOM, we chose its frequency and phase advance so that the mode is synchronised with the beam.

The tables attached at appendix A show the results obtained for all these parameters for the first cell (1), middle cell (11) and last cell (21) calculated with HFSS for the first 20 eigenmodes. All the parameters are calculated on the beam axis. Monopole modes are calculated with perfect magnetic boundary conditions in x and y axis meanwhile dipole modes (which includes also quadruple modes) are calculated with perfect magnetic boundary condition in x axis and perfect electric boundary condition in y axis. These results have been plotted in Fig. 6 (first cell), Fig. 7 (middle cell) and Fig. 8 (last cell) for better comparison. In addition, frequency bands from A to F have been introduced in the monopole modes to support the explanation.

Referring to the results for R/Q we can see that, among the monopole modes, the ones with strongest interaction are A, B, C, D, E and F. Between them, A is the operation mode, which resonates at a frequency of 999.50 MHz. After it, C is the mode with strongest interaction, nevertheless is well detuned as well as all the other bands as can be seen in Fig. 5. A dangerous mode is B, which resonates close to the first machine line at 2.00 GHz. Secondly, related with Q_{SiC}, going back to the comparison between monopole and dipole modes for the three cells, we can see that the monopole modes are almost not damped by the S_iC loads meanwhile the dipole modes are strongly damped by them. This behaviour matches with the one described for the structure with 19 cells and 15.00 MW in [1]. No significant change has been observed with respect to HOM's in the new design therefore we can conclude that they are sufficiently damped and the former beam dynamics analysis is still valid.

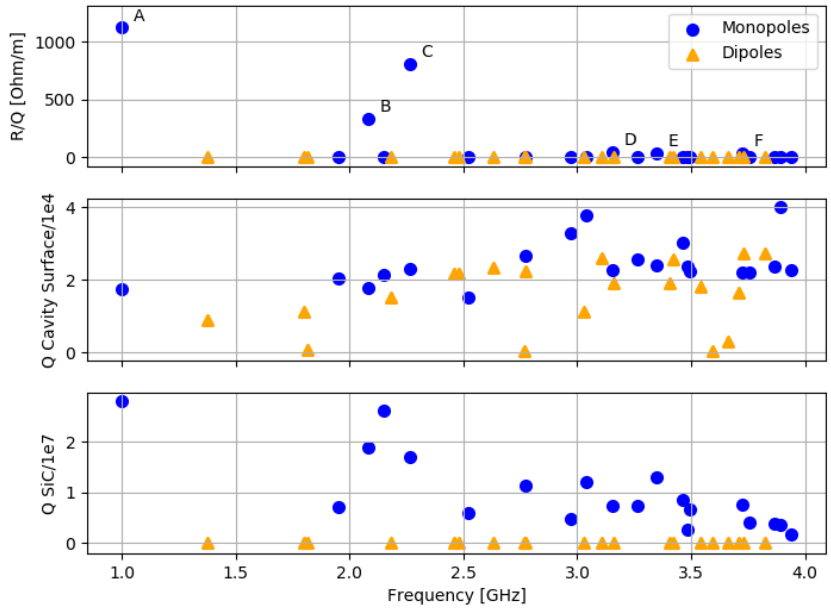

Figure 6: *Comparison of R/Q (up), $Q_{CavitySurface}$ (middle) and Q_{SiC} (bottom) for the monopole and dipole modes in the first cell.*

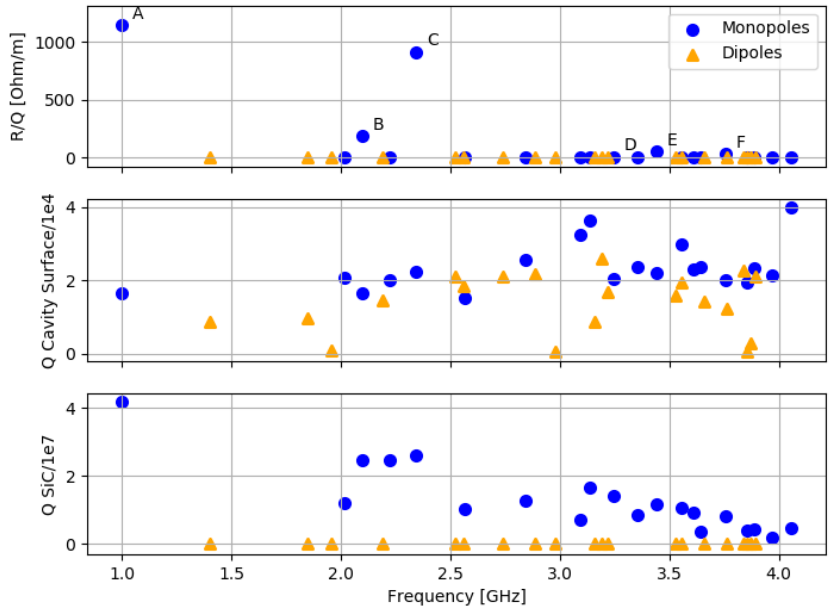

Figure 7: *Comparison of R/Q (up), $Q_{CavitySurface}$ (middle) and Q_{SiC} (bottom) for the monopole and dipole modes in the middle cell.*

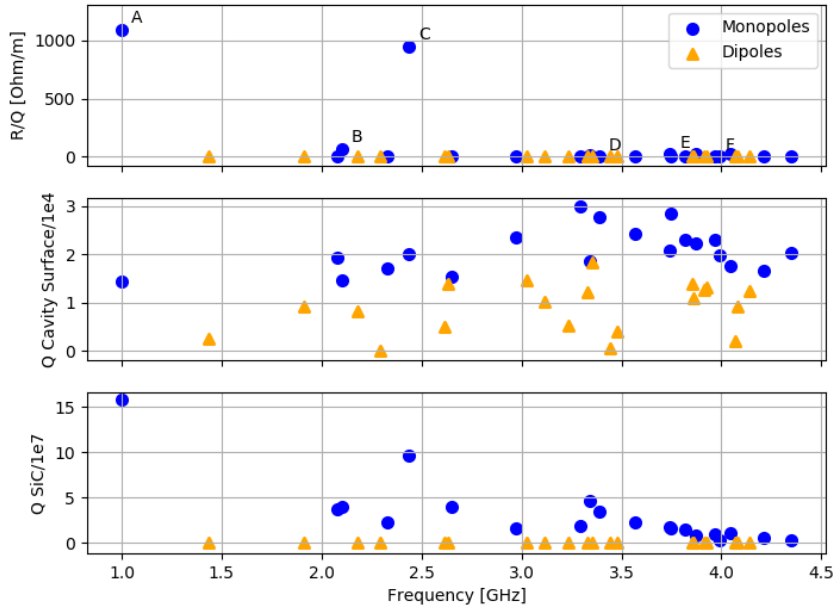

Figure 8: *Comparison of R/Q (up), $Q_{CavitySurface}$ (middle) and Q_{SiC} (bottom) for the monopole and dipole modes in the last cell.*

4 Coupler Design

4.1 Input coupler design

The length of every cell in the TW structure is chosen to set a specific phase advance per cell. In our case this length is 99.98 mm for a phase advance per cell of $2\pi/3$. At the same time, the dimensions of the coupler cell for the TW structure are designed to minimize the power reflections at the input or output ports.

With the electromagnetic simulation codes is not possible to simulate just the

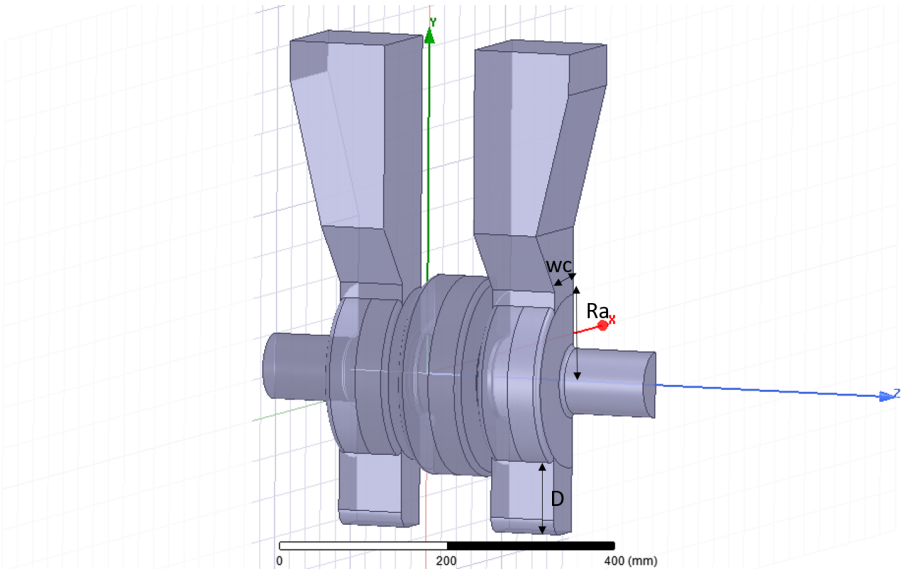

Figure 9: *HFSS model used to perform the optimization of the couplers. On this case, the input coupler behaves as input and output coupler. Adjusting R_a, w_c and D it is possible to reduce both the input reflection and the dipole-kick's.*

coupler with the boundary conditions that matches the TW with a finite number of cells behaviour. One possible way to perform the optimization would be to simulate the input and the output coupler with few cells in between, and optimize them to minimize the coefficient of reflection at the input. But, instead of reaching a zero reflection coefficient due to the cancellation between the waves reflected at the input and output couplers, the backward wave found in the structure can affect the phase advance. This problem is described in depth in [10], together with a method of optimization, taking into account the phase advance.

Main requirements for the design of the coupler are a reflection S_{11} at the operating frequency of 999.50 MHz lower than -30.00 dB. In addition, at a bandwidth of 1.00 MHz from the operating frequency, the reflection has to be kept lower than -30.00 dB as well. At the same time, the phase advance per cell can not change from $2\pi/3$.

The first method described in [10], where the radius of the coupler cell and the input aperture are tuned in order to reduce the input reflection and keep a stable phase, was tested. The results of this optimization were satisfactory both in phase advance and reflection. But, since the optimization is performed with three different simulation files, this makes the convergence of the optimization less reliable and harder to automate. Furthermore, while analysing the dipole's kick effect inside the coupler, an off-set on the beam axis field was detected Fig. 10a. Therefore, it was necessary to introduce a short-end at the bottom of the cavity [11] in order to reduce the dipole-kick value and, consequently, the beam's offset. In Fig. 10 it can be seen how the field off-set is reduced by just adding this short-end to the coupler. This increased the optimization parameters to the radius of the coupler's cell, the input aperture and the short-end length. These parameters are marked in Fig. 9 as w_c (input aperture), R_a (cell radius) and D (short-end length).

For this reason, the new optimization process is performed in a model with the

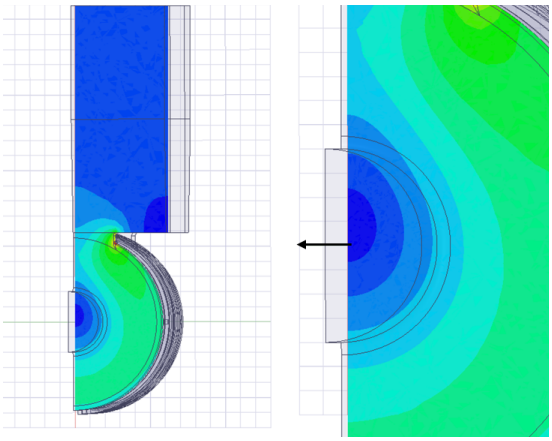

(a) *Coupler without short-end. An off-set of the fields on the beam axis (black arrow) is visible.*

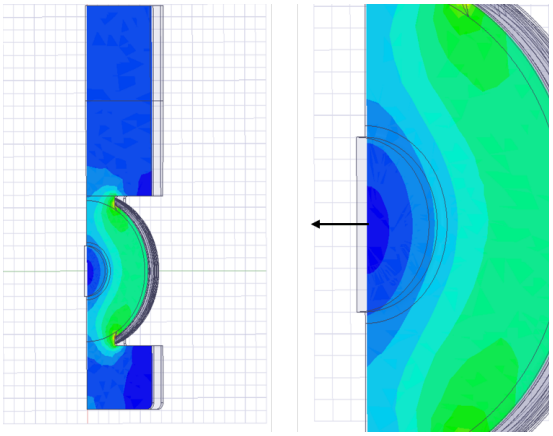

(b) *Coupler with short-end. Adjusting its length is possible to reduce the dipole-kick's value.*

Figure 10: *Comparison between the field at the beam axis with and without short-end.*

input coupler, working at the same time as input and output coupler, with the first cell in between Fig. 9. The point is to tune w_c and R_a to minimize the S11 value at 999.50 MHz when, in between the two couplers, we use one, two or three identical cells. Doing this we obtained the polar plot shown in Fig. 11a where the vertex of every triangle represents the S_{11}, for a determined R_a and w_c, when the model has the first cell once, twice or three times in between the couplers.

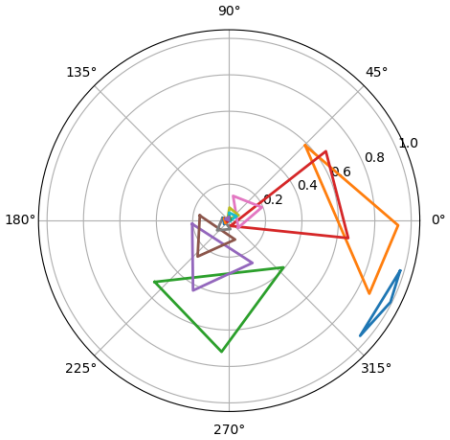

(a) *Polar plot of S_{11} values at 999.50 MHz. Tuning process of R_a and w_c.*

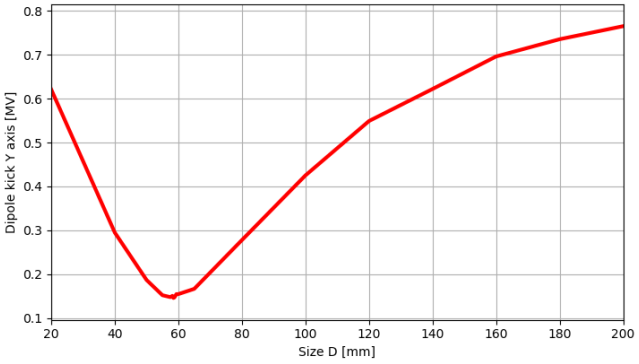

(b) *Example of optimization of dipole-kick's by tuning D.*

Figure 11: *Iterative two steps optimization process of R_a, w_c and D. On the left, every vertex of each triangle represents the S_{11} with one, two or three cells in between the two couplers.*

Once the optimization of the values R_a and w_c is done, we proceed to tune D to get a proper value for the dipole-kick. On Fig. 11b is represented how the dipole-kick changes while D increases its length. The dipole-kick parameter reaches its maximum when D is 20.00 mm and slowly decreases to a minimum at 60.00 mm,

and then continues increasing until it finally saturates at 200.00 mm. This change in D will produce an increase in the reflection, so we have to tune again the values of R_a and w_c. This leads to an iteration process which finished converging to the optimum values of R_a, w_c and D, minimizing both the dipole-kick and the reflection.

The final result of the tuning can be seen in Fig. 12 for the reflection and in Fig. 13 for the phase advance and field amplitude for the example with three cells. With this process, we managed to reach an S_{11} of -48.46 dB at 999.50 MHz and a phase advance per cell of $2\pi/3$.

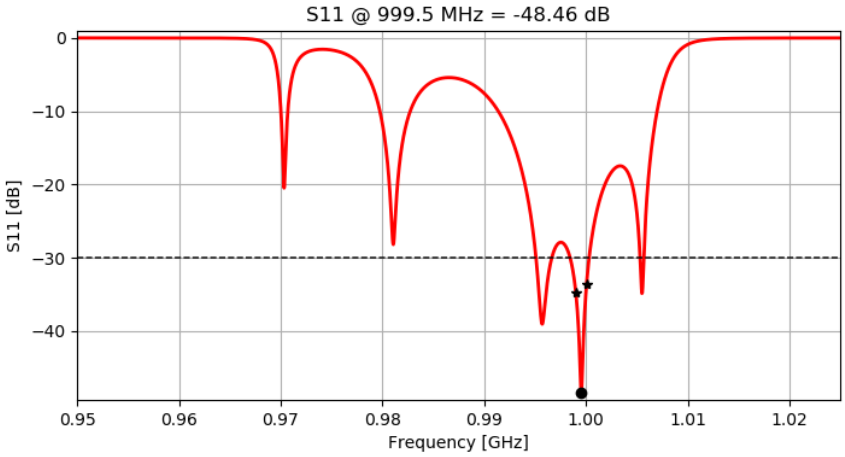

Figure 12: *Reflection at the input coupler of a 3 cell setup.*

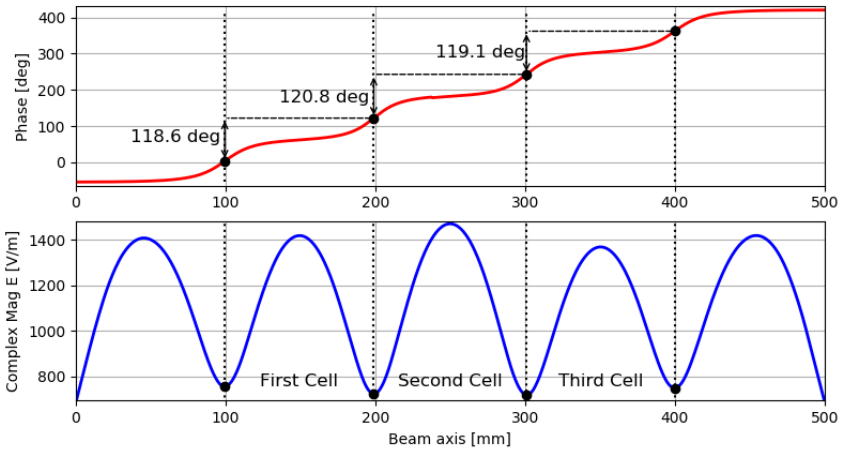

Figure 13: *Phase advance per cell and field amplitude after input coupler's optimization with three cells.*

4.2 Output coupler design

The same simulations as for the input coupler were performed. But in this case, the optimization of R_a, w_c and D was not converging to an optimum. Convergence studies were performed and the results can be found in Fig. 14 where some fluctuations on the last steps are noticeable.

Even though the optimization of the input coupler was successful, the output coupler is characterized by its really low group velocity. This characteristic, makes

the output coupler more sensitive to the frequency error. This may come from the numerical convergence in terms of passes over the adaptive mesh convergence or from the geometry description or surface mesh quality. The surface mesh describing the geometry is generated at the beginning of the simulation and it does not improves with the passes.

For the context of this report, and on the next sections, we have assumed as optimum the last value obtained on the optimization. However, we consider necessary to carry out further studies about the influence of the frequency and the low group velocity on the numerical convergence of the optimization.

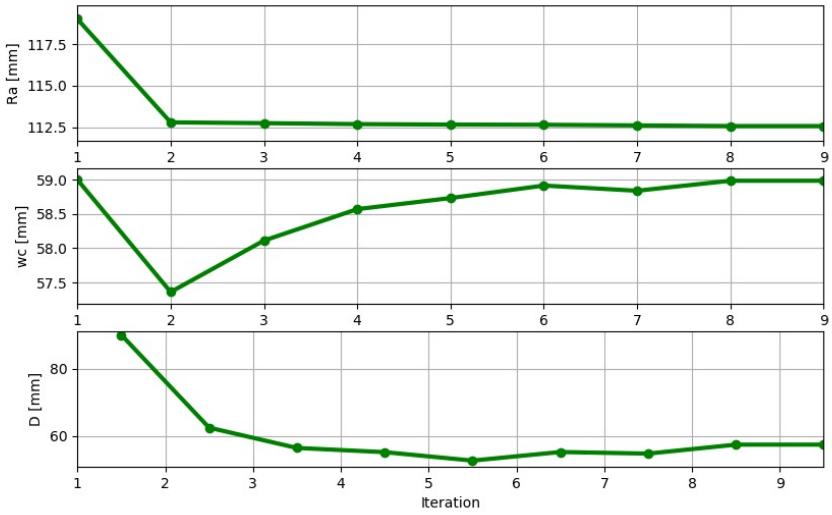

Figure 14: *Convergence studies of output coupler's dipole-kick optimization process.*

5 PLACET simulations

The influence of the designed structure on the drive beam has been studied with the tracking code PLACET. The code takes into account the most prominent higher order modes using the calculated shunt impedance's and quality factors. In addition the dipole kicks of the couplers due to the non-perfect compensation of the coupler asymmetry are introduced. Those kicks have been simulated by a zero-length RF-dipole cavity [12].

The simulations showed that no significant emittance growth is to be expected from neither the higher order modes nor the dipole-kicks of the couplers. Alternating the coupler orientation by 90.00 deg even further reduces the effect. The results are shown in Fig. 15 for the second drive beam accelerator in the horizontal and vertical plane. The coupler fields seem to be well compensated since the actual dipole filed amplitude on axis has to be increased by a factor 1000 to see a significant effect in the simulations. The relative large aperture of the structure seem to lead to this insensitivity.

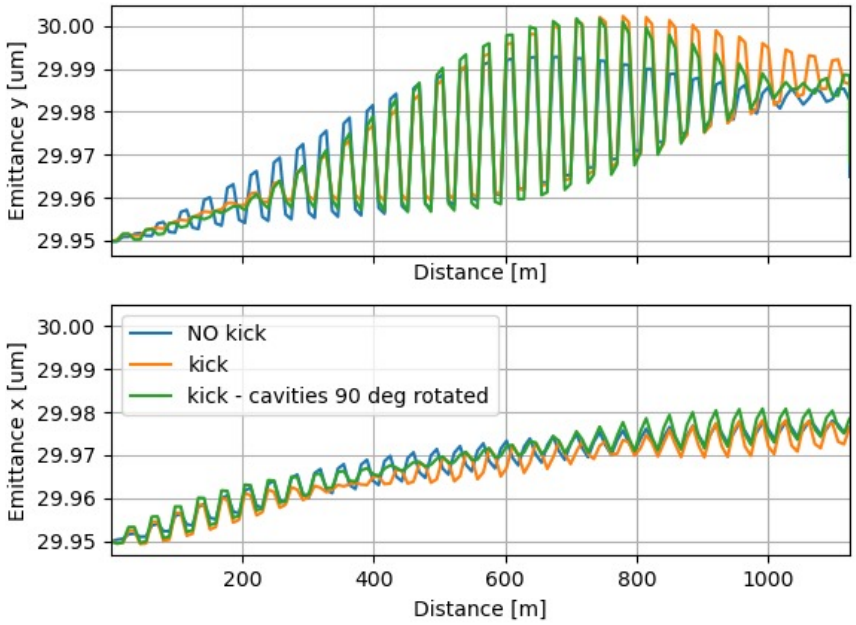

Figure 15: *Emittance evolution along the DBL taking into account coupler kicks and the possibility to rotate every second coupler by* 90.00 deg.

6 Conclusion

The design of the fully loaded CLIC drive beam accelerating structure has been updated taking into account the higher klystron power available. The new structure has two more cells and maintains the extremely high RF to Beam efficiency of 99% and the filling time of 245.00 ns. An input and output coupler with dipole field compensation has been designed and optimised for the structure. The methods to optimize the cells of the structure and the couplers have been described. Finally beam dynamics simulations have been performed with the tracking code PLACET to verify that the higher order modes found are sufficiently damped and not harmful for the CLIC drive beam. The dipole-kick of the couplers have been simulated as well in PLACET and it was shown that their influence is negligible for the current design.

7 Acknowledgement

The authors like to thank R. Wegner and A. Grudiev for their advice concerning the RF simulations and A. Latina and R.A. Janeiro Costa for their help with PLACET.

A HOM data tables

Table 1: *Monopole modes First Cell.*

Band	f_{syn}(GHz)	ϕ_{syn} (°)	R/Q (Ω/m)	$Q_{\text{CavitySurface}}$	Q_{SiC}
A	0.9997	120.00	1119.40	17352	2.8138×10^7
	1.9517	125.50	0.00	20573	7.2420×10^6
B	2.0828	109.10	332.30	17716	1.8954×10^7
	2.1492	101.80	0.00	21442	2.6138×10^7
C	2.2655	87.30	803.20	23173	1.7014×10^7
	2.5195	58.20	0.00	15282	6.0762×10^6
	2.7733	27.30	0.00	26757	1.1283×10^7
	2.9702	3.60	0.00	33015	4.8709×10^6
	3.0416	5.50	0.00	37710	1.2150×10^7
D	3.1561	18.20	50.10	22746	7.2857×10^6
	3.2667	32.70	0.00	25699	7.4324×10^6
E	3.3496	41.80	32.30	23980	1.2989×10^7
	3.4614	54.50	0.00	30199	8.4882×10^6
	3.4858	58.20	0.00	23582	2.7014×10^6
	3.4941	58.20	0.00	22274	6.6156×10^6
F	3.7254	87.30	36.80	22183	7.5193×10^6
	3.7581	90.90	0.00	22181	4.1690×10^6
	3.8665	103.60	0.30	23585	3.7513×10^6
	3.8938	107.30	0.00	40066	3.5937×10^6
	3.9387	112.70	0.00	22613	1.7743×10^6

Table 2: *Monopole modes Middle Cell.*

Band	f_{syn}(GHz)	ϕ_{syn} (°)	R/Q (Ω/m)	$Q_{\text{CavitySurface}}$	Q_{SiC}
A	0.9996	120.00	1142.80	16432	4.1931×10^7
	2.0141	118.20	0.00	20733	1.1918×10^7
B	2.0964	109.10	185.20	16642	2.4471×10^7
	2.2251	92.70	0.00	19910	2.4664×10^7
C	2.3417	80.00	907.00	22356	2.5872×10^7
	2.5675	50.90	0.00	15298	1.0367×10^7
	2.8439	18.20	0.00	25732	1.2549×10^7
	3.0940	10.90	0.00	32396	6.9900×10^6
	3.1390	16.40	0.00	36260	1.6659×10^7
D	3.2439	29.10	2.40	20384	1.4100×10^7
	3.3526	41.80	0.00	23549	8.5569×10^6
E	3.4400	52.70	52.30	22070	1.1591×10^7
	3.5584	67.30	0.00	29728	1.0557×10^7
	3.6092	72.70	0.00	22912	9.3068×10^6
	3.6446	76.40	0.00	23788	3.7060×10^6
F	3.7559	90.90	30.50	20171	8.2498×10^6
	3.8541	101.80	0.00	19342	4.0524×10^6
	3.8871	105.50	0.00	23208	4.3869×10^6
	3.9695	116.40	0.00	21393	1.9501×10^6
	4.0564	127.30	0.00	39936	4.5851×10^6

Table 3: *Monopole modes Last Cell.*

Band	f_{syn}(GHz)	ϕ_{syn} (°)	R/Q (Ω/m)	$Q_{\text{CavitySurface}}$	Q_{SiC}
A	0.9995	120.00	1088.80	14413	1.5842×10^8
	2.0801	110.90	0.00	19303	3.6763×10^7
B	2.0997	107.30	67.20	14622	3.9417×10^7
	2.3315	80.00	0.00	17095	2.2573×10^7
C	2.4377	67.30	944.80	20137	9.6787×10^7
	2.6526	41.80	0.00	15395	4.0301×10^7
	2.9738	3.60	0.00	23527	1.6592×10^7
	3.2936	34.50	0.00	29817	1.8544×10^7
D	3.3396	41.80	11.50	18675	4.5854×10^7
	3.3872	45.50	0.00	27752	3.5060×10^7
	3.5668	67.30	0.00	24343	2.3233×10^7
E	3.7412	89.10	19.60	20722	1.7690×10^7
	3.7497	89.10	0.00	28322	1.6264×10^7
	3.8207	98.20	0.00	23011	1.4334×10^7
F	3.8727	103.60	29.00	22198	8.5717×10^6
	3.9690	116.40	0.00	22956	1.0048×10^7
	3.9921	118.20	0.00	19858	3.2124×10^6
	4.0446	125.50	19.80	17516	1.0191×10^7
	4.2115	145.50	0.00	16573	5.2323×10^6
	4.3491	161.80	0.00	20206	2.6455×10^6

Table 4: *Dipole modes First Cell.*

$freq_{syn}$(GHz)	phi_{syn}(°)	$R/Q(\Omega/\mathrm{m})$	$Q_{CavitySurface}$	Q_{SiC}
1.3758	165.5	0.1	8816	41
1.8010	143.6	7.2	11353	96
1.8143	140.0	2.5	633	2
2.1822	98.2	2.0	15014	196
2.4572	65.5	1.5	21594	508
2.4775	61.8	0.1	1822	401
2.6301	43.6	0.0	23479	625
2.7673	23.6	0.0	507	2
2.7741	27.3	0.5	22404	4408
3.0305	3.6	2.1	11341	49
3.1094	12.7	0.0	26132	4024
3.1611	20.0	0.0	19040	297
3.4041	49.1	0.0	19182	689
3.4219	50.9	0.5	25635	181
3.5398	65.5	0.0	18009	79
3.5931	76.4	0.6	513	2
3.6609	83.6	0.0	3108	4
3.7087	85.5	0.0	16528	90
3.7283	87.3	0.0	27240	349
3.8253	98.2	0.0	27346	2018

Table 5: *Dipole modes Middle Cell.*

$freq_{syn}$(GHz)	phi_{syn}(°)	$R/Q(\Omega/\mathrm{m})$	$Q_{CavitySurface}$	Q_{SiC}
1.4044	169.1	0.2	8608	38
1.8471	138.2	9.6	9605	75
1.9548	123.6	1.7	721	2
2.1882	98.2	2.1	14436	184
2.5229	56.4	1.4	21108	844
2.5618	52.7	0.0	18337	387
2.7417	30.9	0.0	21020	394
2.8886	12.7	0.0	21665	10788
2.9803	1.8	0.3	602	2
3.1590	18.2	0.7	8717	31
3.1918	23.6	0.0	25864	11005
3.2193	27.3	0.2	16817	256
3.5288	63.6	0.1	15704	288
3.5578	67.3	0.1	19346	150
3.6617	80.0	0.0	14173	56
3.7648	90.9	0.6	12302	109
3.8418	100.0	0.0	22667	1753
3.8552	107.3	0.0	660	2
3.8745	109.1	0.0	2787	4
3.8925	107.3	0.0	21108	197

Table 6: *Dipole modes Last Cell.*

$freq_{syn}$(GHz)	phi_{syn}(°)	$R/Q(\Omega/\mathrm{m})$	$Q_{CavitySurface}$	Q_{SiC}
1.4375	172.7	0.6	2616	7
1.9093	130.9	11.4	9320	46
2.1823	98.2	1.5	8306	145
2.2933	85.5	1.0	123	0
2.6126	47.3	0.6	5092	55
2.6301	43.6	0.0	13849	1551
3.0265	3.6	0.0	14542	40
3.1176	14.5	0.0	10189	200
3.2348	27.3	0.1	5303	18
3.3303	40.0	0.0	12123	37
3.3515	41.8	0.3	18407	24548
3.4449	52.7	0.1	527	0
3.4785	56.4	0.1	4137	2
3.8546	101.8	0.0	13958	7485
3.8617	103.6	0.0	10949	267
3.9124	109.1	0.0	12693	1356
3.9235	110.9	0.0	13150	29
4.0663	127.3	0.0	1967	0
4.0790	129.1	0.0	9215	9
4.1401	136.4	0.0	12384	45

References

[1] Rolf Wegner and Erk Jensen. CLIC drive beam accelerating structures. Technical report, CERN, Geneva, Switzerland, 2012. Available as CLIC-Note-945.

[2] Günther Geschonke and Andrea Ghigo. CTF3 design report. Technical report, CERN, Geneva, Switzerland, 2002. Available as CERN/PS 2002-008 (RF).

[3] Erk Jensen. CLIC Drive Beam Accelerating Structures. In *LINAC 2002*, 2002.

[4] Roberto Corsini. First Full Beam Loading Operation with the CTF3 LINAC. In *EPAC 2004*, 2004.

[5] P.N. Burrows *et al.* Updated baseline for a staged compact linear collider. Technical report, CERN, Geneva, Switzerland, 2016. Available as CERN 2016-004.

[6] Daniel Schulte. Placet: a program to simulate the drive beams. Technical report, CERN, Geneva, Switzerland, 2000. Available as ERN-PS-2000-028-AE, CLIC-Note-437.

[7] Rolf Wegner. CLIC drive beam linac. The Workshop of Future Linear Colliders, 2012.

[8] Avni Aksoy. CLIC drive beam linac optimization. CLIC Workshop, 2018.

[9] E. Jensen. RF Cavity Design. In *CERN Accelerator School: Advanced Accelerator Physics Course*, pages 405–429, 2014.

[10] David Alesini, Alessandro Gallo, Bruno Spataro, Agostino Marinelli, and Luigi Palumbo. Design of couplers for traveling wave RF structures using 3D electromagnetic codes in the frequency domain. *Nucl. Instrum. Meth. A*, 580:1176–1183, 2007.

[11] Seyd Hamed Shaker, Steffen Döbert, Raphael Leuxe, Shahin Sanaye Hajari, and Luca Dassa. Sub-harmonic Buncher Design for the CLIC Drive Beam Injector. In *4th International Particle Accelerator Conference*, page TUPME052, 2013.

[12] A. Latina *et al.* Study of Coupler's Effect on ILC like Lattice. In *IPAC 2010*, 2010.